Tribology International 189 (2023) 108963

Contents lists available at ScienceDirect

Tribology International

journal homepage: www.elsevier.com/locate/triboint

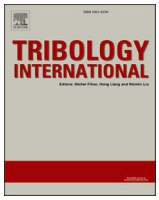

An insight into the effect of rough surfaces and contact orientation on the fretting characteristics of quenched and tempered steel

A. Zabihi [a,*], J. Juoksukangas [b], J. Hintikka [c], M. Honkanen [d], A. Mäntylä [c], J. Vaara [c], T. Frondelius [c], M. Vippola [d]

[a] Tribology and Machine Elements, Materials Science and Environmental Engineering, Faculty of Engineering and Natural Sciences, Tampere University, P.O. Box 589, 33014 Tampere, Finland
[b] Machine Design, Automation Technology and Mechanical Engineering, Faculty of Engineering and Natural Sciences, Tampere University, P.O. Box 589, 33014 Tampere, Finland
[c] R&D and Engineering, Wärtsilä Finland Oy, P.O. Box 244, 65101 Vaasa, Finland
[d] Tampere Microscopy Center, Tampere University, P.O. Box 692, 33014 Tampere, Finland

ARTICLE INFO

Keywords:
Fretting
Rough Surfaces
Friction
Adhesion

ABSTRACT

The effect of a rough, textured surface and contact orientations on the fretting behavior of self-mated martensitic 34CrNiMo6 +QT steel was examined via a large annular flat-on-flat contact. A friction study accompanied by microscopy analyses was performed to provide a clear insight into fretting characteristics. In gross sliding, the rough surface revealed a lower delayed friction peak and the same steady-state friction as the fine-ground smooth one. In partial slip, the stable friction threshold was around 0.5 for both surfaces. The oxidation-abrasion and its combination with adhesion were observed as wear mechanisms in partial slip and gross sliding, respectively.

1. Introduction

In industrial machinery, a micrometer-level oscillatory slip is termed fretting, which gives rise to an early failure below the plain fatigue limit and leads to fatigue and wear. It is verified that the non-idealities in friction, fretting fatigue, and wear make the estimation of fretting fatigue life more demanding [1]. In terms of running conditions, the contacts can be exposed to partial slip (some areas are stuck while others slip), gross slip (no sticking), or a mixed slip regime [2–4]. An adhesive peak of coefficient of friction (COF) due to the localized tangential traction in fretting increases (sub)surface stresses and nucleates cracks [5], dramatically declining fatigue life. In engine parts with large contact interfaces, fretting-induced cracking occurred under the adhesion spot at 20% of the fatigue limit owing to the high stress concentration [6].

The existence of non-Coulomb friction is proved in fretting contact configurations and material pairs [7–9]. However, the Amonton/ideal Coulomb friction law is still utilized because friction is not a well-understood phenomenon. In gross slip conditions via quenched and tempered steel, COF developed quickly and peaked at a value of nearly 1.4 at the early stages of the test. Then, it declined gradually and stabilized at a value of around 0.7 [10,11].

Besides, fretting wear as a result of surface sliding can be characterized by surface degradation, e.g., material transfer and wear debris in the contact [12]. As reported by the literature, wear is a contributing factor in the distribution of slip and contact stresses [13,14]. It is substantiated that fretting wear can extend fatigue life by increasing contact size, reducing contact pressure, relocating the points under the most severe stresses [15], and removing newly nucleated cracks. In contrast, fretting wear can lead to the loosening of the real machine components under partial slip and joint failure [6]. Third body particles and layers originating from wear can contribute to wear and friction using velocity accommodation mechanisms as the load-carrying parts [16]. Additionally, their role is essential in fretting owing to the micrometer-level slip amplitude and closed contact under fretting circumstances [17]. Accordingly, any modification to the contact geometry in favor of friction and wear (the formation and ejection of third bodies) might be a beneficial accomplishment.

Large-scale flat-on-flat contacts are normally used in industry, where the applied dynamic load on the assembled parts and vibrations can produce small movements compared to their contact size, which is not a preferred condition. The micro to millimeter-scale cracks, primarily

* Corresponding author.
E-mail address: amirhossein.zabihi@tuni.fi (A. Zabihi).

https://doi.org/10.1016/j.triboint.2023.108963
Received 12 January 2023; Received in revised form 31 July 2023; Accepted 16 September 2023
Available online 19 September 2023

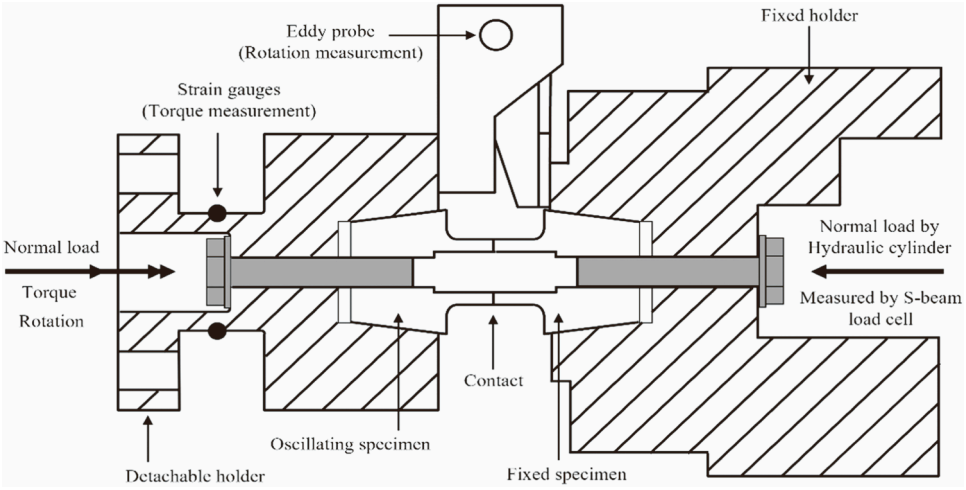

Fig. 1. A schematic view of fretting test device configuration.

beneath adhesion spots, and wear induced by fretting in such contacts [18], can impair the functionality of the joint assembly. Thus, the improvement of the surface geometry, as an effective factor in contact stress distributions, cracking, friction, and wear, is vital to avoid a catastrophic fretting failure.

A textured surface is referred to as a rough surface with a regular pattern, which could be made via machining or electro-polishing [19] and is rarely utilized in fretting experimental literature. Vázquez et al. [20] stated that a wavy surface texture enhances fretting fatigue life through the re-distribution of the stress and strain fields on the surface. K.J. Kubiak et al. [21] realized that higher initial surface roughness can increase wear rate and reduce COF under the gross sliding fretting regime. The different surface roughnesses made by the particular machining processes were studied in other investigations, signifying a strong correlation between the roughness and fretting-induced friction and wear, specifically in the transition from partial slip to full sliding [22,23]. Also, contact geometry was proposed by A.R. Warmuth et al. [24] as a critical factor in the rate and mechanism of fretting wear. It was asserted that the less the conforming contact, the higher the fretting wear rate and the lower the adhesion. A. Beheshti et al. [25] proposed a notable deviation of the contact pressure and tangential traction distributions from the Hertzian condition as a result of high surface roughness and a low normal load. In addition, the influence of roughness on the frictional shear stress has been modelled by W. Qin et al. [26], resulting in discrete, time-dependent, and highly concentrated shear stresses for a rough surface compared with a smooth one.

Following the aforementioned statements, surface texture controls contact mechanics as one of the crucial factors in fretting failure. In this regard, an investigation into the impact of a textured rough surface on the fretting response of quenched and tempered steel was carried out using a large flat-on-flat contact to be more analogous to practical engineering applications.

The main aim of this study was to gain fundamental knowledge of the role of surface roughness in the fretting performance of a large annular flat-on-flat contact with a unique surface texture, which has not previously been assessed in the literature. The primary objective was to research rough-rough contacts with two texture orientations in the partial and gross slip fretting regimes and compare with smooth-smooth contacts to ascertain if they could improve fretting-induced friction, wear, and cracking.

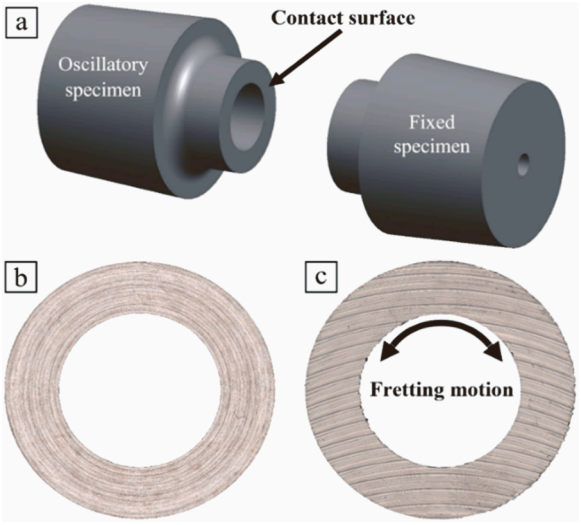

Fig. 2. (a) 3D view of fretting test specimens, Alicona optical profilometry images of (b) smooth and (c) rough surfaces.

2. Experimental

2.1. Materials and test device

Quenched and tempered steel specimens (EN 10083–1–34CrNiMo6 +QT) were employed in the experiments as the self-mated pairs. The hardness of the test specimens was 341 ± 15 HV with an applied load of 500 g and dwell time of 10 s, measured by an MMT-X7 Matsuzawa Vickers tester according to ASTM E92–17. A large annular flat-on-flat contact apparatus was utilized to carry out fretting tests. It was designed and fabricated in-house, and detailed information on the test device and procedure can be found elsewhere [11]. Using a larger contact rather than a conventional lab-scale device with a small Hertzian contact can provide a more comprehensive study on fretting damage. As a brief description, two tubular fretting specimens were pressed against each other by a normal load applied using a hydraulic cylinder to form an axisymmetric flat-on-flat contact configuration. One specimen was fixed in place, and the other oscillated via an electric shaker attached using a lever arm to the holder to generate a rotational slip. The rotation was linearly increased from zero to the target value after 400 load cycles; this period is called the start-up phase. A schematic view of the test device configuration is illustrated in Fig. 1.

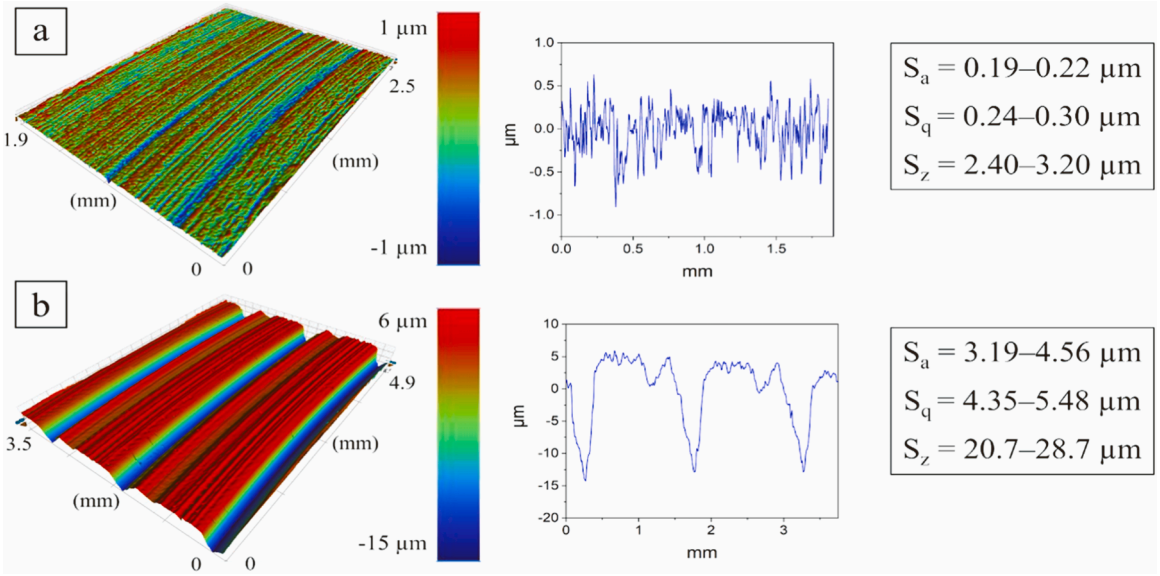

Fig. 3. 3D topography on the left, 2D surface profile in the middle, and surface roughness parameters of (a) smooth and (b) rough surfaces.

Table 1
The annular flat-on-flat fretting test matrix.

Test No.	Series name	Load cycles (N_{LC})	Sliding amplitude (u_a) [μm]	Specimen orientation
1	Gross sliding	3×10^6	35	-
2	Gross sliding	3×10^6	35	Parallel
3	Gross sliding	3×10^6	35	Perpendicular
			TRM level [-]	
4	Stable friction	3×10^6	0.40	Parallel
5	Stable friction	3×10^6	0.50	Parallel
6	Stable friction	3×10^6	0.61	Parallel
7	Stable friction	3×10^6	0.53	Perpendicular
8	Stable friction	3×10^6	0.57	Perpendicular

2.2. Contact geometry

Test specimens were shaped by turning a rod with a diameter of 45 mm. The smooth and rough contact surfaces were manufactured via fine-grinding and milling, respectively. Fig. 2 presents the test specimens and optical profilometry images of the smooth and rough surfaces (acquired by an Alicona InfiniteFocus G5 model 3D optical profilometer). The circular grinding scratches on the smooth surface and the grooves on the rough one can be seen.

The surface roughness parameters (Sa; arithmetical mean height, Sq; root mean square height, Sz; maximum height), along with 3D topography and 2D profiles of the surfaces, measured by the Wyko NT1100 optical profiling system, are presented in Fig. 3.

The annular tube area is 314 mm^2, with inner and outer radii of 7.5 and 12.5 mm, respectively. It can be said to be the nominal contact area in the smooth surfaces, but not in the rough surfaces if we consider the grooves not to be part of the nominal area. This surface pattern was achieved via a high-precision milling machine (GF Mikron Mill P 800 UD), and approximately the same groove depth and spacing (about 16 grooves on the surface) can be observed according to Figs. 2 and 3.

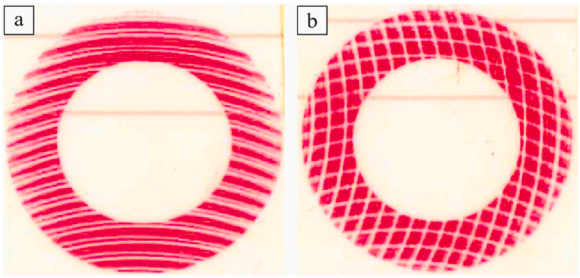

Fig. 4. The surface pressure distribution on the rough surfaces; (a) parallel and (b) perpendicular contact orientations.

2.3. Fretting test matrix

The test parameters are listed in Table 1, in which the nominal contact pressure of 30 MPa and loading frequency of 40 Hz were applied in all fretting tests, which were selected based on the comprehensive earlier published experiments with the smooth surface [18,27]. Two test types were carried out at ambient temperature and relative humidity, including gross sliding and so-called stable friction. The whole contact is subjected to slip in gross sliding as a result of its having sufficient sliding amplitude. The stable friction test is associated with applying a limited amount of cyclic tangential load. Thus, it was conducted to ascertain a threshold above which instability is seen in the frictional behavior [11]. In fact, COF can apply to gross sliding but not to partial slip. Hence, traction ratio (TR=tangential traction/normal traction), equivalent to COF in gross sliding, was employed to study the frictional properties under stick or partial slip [28]. Table 1 presents the sliding amplitude and maximum traction ratio (TRM) in the gross sliding and stable friction tests, respectively. It should be remarked that two types of contact, including smooth-smooth and rough-rough, were studied in this investigation and the smooth contact has already been tested several times for both test types [11,28,29]. Besides, the gross sliding tests were performed three times for the rough-rough cases to ensure acceptable repeatability.

In addition to comparing the smooth and rough specimens, the influence of the different contact orientations on fretting characteristics was considered in the rough cases. For this purpose, the grooves were positioned one against another in the parallel and perpendicular orientations, as demonstrated in Fig. 4. Subsequently, the specimens were

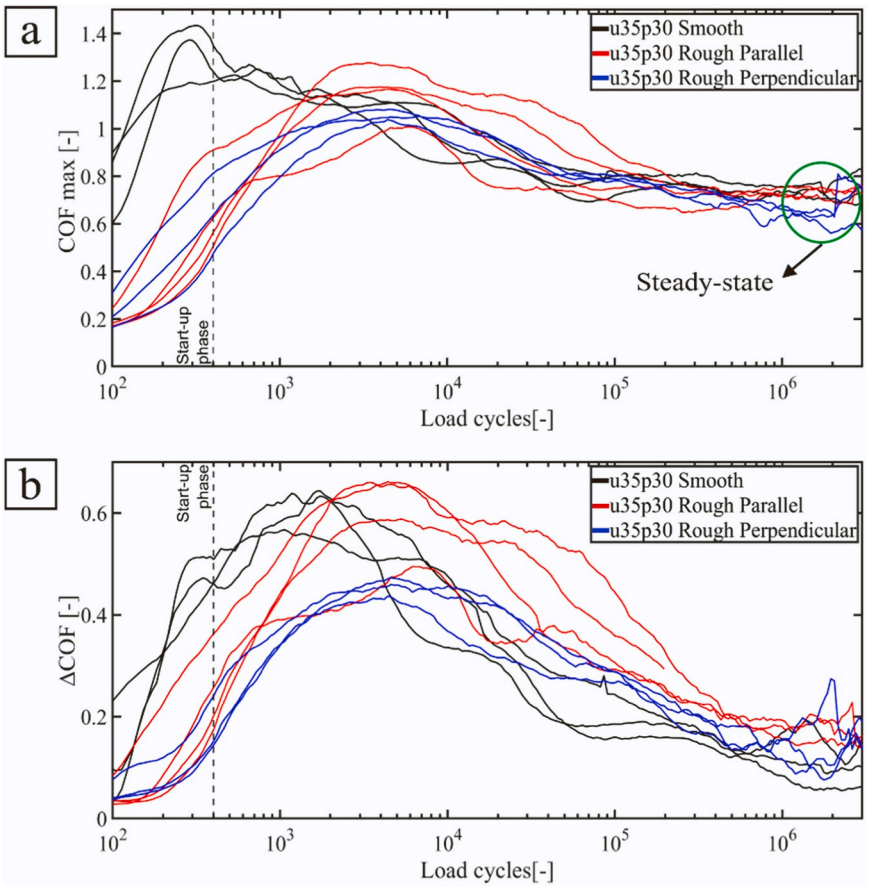

*One parallel-oriented rough surface test with 2×10^5 cycles is included in the figure to use its COF peak data.

Average / Contact	COF (Peak)	Peak cycle (N_{LC})	COF (Steady-state)	Accumulated sliding distance (m)
Smooth	1.35	379	0.73	433.25
Parallel	1.15	4423	0.73	430.94
Perpendicular	1.05	5270	0.65	428.77

Fig. 5. (a) COFmax and (b) ΔCOF curves under gross sliding; u: sliding amplitude - p: normal pressure (the vertical dotted line at 400 load cycles shows the duration of the start-up phase).

aligned using the pressure-sensitive film (Fuji Prescale) in order to ensure an even nominal surface pressure distribution and correct orientation.

2.4. Characterization methods

Ultrasonic cleaning of the test specimens was conducted with acetone and then ethanol before and after each test. The unfretted and fretted specimens were weighed using a Precisa EP 420 A model laboratory balance with the readability down to 0.1 mg to calculate wear mass loss. Each specimen was scaled five times via a reference sample, and next the average value was reported as mass loss. The whole surface was imaged by a Leica MZ75 stereomicroscope and an Alicona 3D optical measurement system to examine the surface damage. Afterwards, the most severely damaged areas were selected for further study since the highest level of fretting fatigue-induced cracks and degradation layers most likely exist there.

Moreover, an SEM microscope (JEOL JSM-IT500) equipped with an energy-dispersive X-ray spectrometer (EDS, JEOL Dry SD30) was utilized to characterize fretting damage. Prior to the cross-sectional studies, the sample preparation was executed by grinding, polishing with 1 μm diamond suspension, and etching through 4% Nital etchant for a period of around 20 s

3. Results and discussion

In this section, the effect of the rough surface and contact orientations on the frictional behavior was linked to the surface damage, degradation layers, and cracking through the analysis of the fretting test data and damage characterization. It can be expected that the major fatigue cracks and material changes occur within or adjacent to the most severely damaged areas or adhesion spots because of highly concentrated tangential traction, and therefore, they were selected for further characterization [18].

3.1. Gross sliding tests

As mentioned in Section 2.3, the first test series was implemented under a gross sliding regime with tangential slip-controlled loading, and slip was kept constant at around 35 μm through the test duration. As shown in Fig. 5a, the COF peaks for the rough surfaces were lower than those for the smooth ones and occurred after a higher number of cycles.

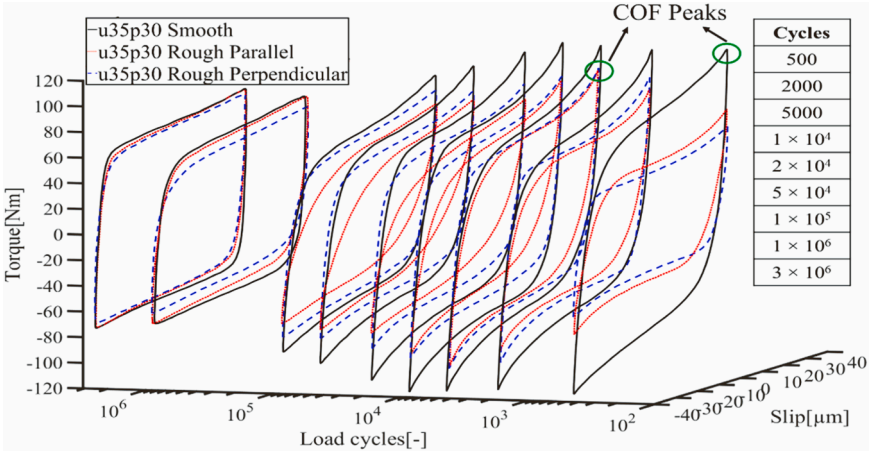

Fig. 6. Fretting loops at different load cycles over the test duration under gross sliding.

The average values of COFs and accumulated sliding distance are listed in the table appended to Fig. 5. Besides, the average friction peak was relatively reduced from the parallel to perpendicular contact orientation.

The initial friction peak represents the adhesion strength in the fretting contact; thus, the severer adhesion spots and cracking are expected to be found in the smooth surface with a higher peak. Nonetheless, the steady-state step, which was considered from 1×10^6 to 3×10^6 cycles, produced nearly the same average COF values of about 0.7 for both textures and contact orientations. It should be mentioned that the start-up phase yields a total of 0.0067% of the accumulated sliding distance occurring after 3×10^6 load cycles; thus, its role is assumed to be insignificant.

As illustrated by Leidich et al., the maximum COF for 34CrNiMo6 +QT against 16MnCr5E in an annular flat-on-flat contact ranged from 1.2 to 1.6 with the same normal contact pressure as our research [30]. Iwabuchi demonstrated a steady-state COF of roughly 0.8 under gross sliding using S45C steel with a cylinder-on-flat contact [31]. Furthermore, Hintikka et al. presented a steady-state COF of 0.8 subsequent to a maximum COF ranging from 1.5 to 1.6 in gross sliding with a self-mated 34CrNiMo6 +QT pair and sphere-on-plane contact [10]. It was also reported that COF at peak and steady-state step for 34CrNiMo6 +QT smooth contact, tested by the same parameters and device as this study, were around 1.4 and 0.7, respectively [27,32]. Hence, our results closely correspond to the previous research.

Fig. 5b demonstrates ΔCOF, which is a difference between the maximum COF calculated from the maximum torque at the extreme end of each fretting cycle and the average COF calculated by the frictional energy dissipation [32]. It can be employed as one of the criteria to apprehend non-Coulomb friction behavior. Accordingly, the higher the ΔCOF, the more the non-Coulomb friction, signifying more interfacial adhesion and adhesive wear.

ΔCOF peaked at the beginning, followed by a decline to a low-value level at the end. It closely agreed with the COF trend, explaining the running-in and steady-state steps. The early ΔCOF values were higher in the smooth surface, showing more deviation from ideal Coulomb friction and adhesive wear. Nevertheless, all surfaces ultimately reached roughly the same low values, which reveal ideal Coulomb friction and abrasive wear.

Given the interface study, two assumptions could be made to rationalize the transition from the COF peak to the stabilized value as follows:

1. The gradual progression of fretting generates the particles resulting in fretting wear, and wear debris abrades the protrusions and depressions and mitigates the asperities' interaction.
2. The development of the third body layers (TBL), owing to the accumulation of wear particles in the interface, can separate the contacts and reduce the initial contact bodies' interactions via velocity accommodation mechanisms [33].

The friction peak was decreased and delayed from a few hundred cycles for the smooth surfaces to a few thousand load cycles for the rough ones. Such that, the COF curves showed an evident difference at the early stage of the tests and then approached together. In the smooth case [11], crossing the initial adhesion peak and achieving steady-state friction may rely on generating a sufficient amount of wear particles. It can take place after a specified distance of accumulated sliding, which is a must for the formation of TBL to accommodate surface sliding and reduce the interaction of the first bodies. The aforementioned procedure is known as a transition from adhesive to abrasive wear. Hence, the contact in the smooth case was firstly adhesive and then oxidative-abrasive. The following reasons could explain the different frictional behavior of the rough surfaces compared with the smooth ones. Firstly, the real contact area was smaller in the rough cases, causing less locally deformed sites [23]. Therefore, the tangential force due to the plastic deformation in the interface was lower than for the smooth case, resulting in lower COF peaks and slower evolution of friction, particularly at the first few thousand cycles. Second, the contact geometry was changed from more conforming to less conforming contact by using this texturization, and fretting wear mechanism tended to be more abrasive (material removal) than adhesive (plastic deformation or material transfer) [24]. Lastly, another possible rationalization can be derived from the so-called "contact oxygenation" concept [34]. Accordingly, the wear mechanism and rate can be determined by oxygen diffusion into the contact such that oxidative-abrasive wear occurs when the interfacial di-oxygen partial pressure exceeds a threshold. This can successfully describe the size of abrasive and adhesive wear areas in the experiments with square and circular flat-on-flat contacts with plain and textured surfaces [35–37]. It elucidates that the di-oxygen partial pressure is maximum at the contact edges next to the atmosphere and reduces as a function of distance from the edge, causing a transition from oxidative-abrasive to adhesive wear. It was asserted that the interface properties and debris expulsion govern oxygen penetration. Therefore, the grooves on the rough texture could assist oxygen ingress and debris ejection, and then oxidative-abrasive wear in the first few thousand cycles, which reduced the COF peak relative to the smooth surface. Consequently, the rough contact was exposed to both oxidative-abrasive and adhesive wear from the early stage of the fretting test, in which adhesion was the dominant wear mechanism early on and abrasion was the one later on.

Fretting loops can provide more detailed information on friction, for

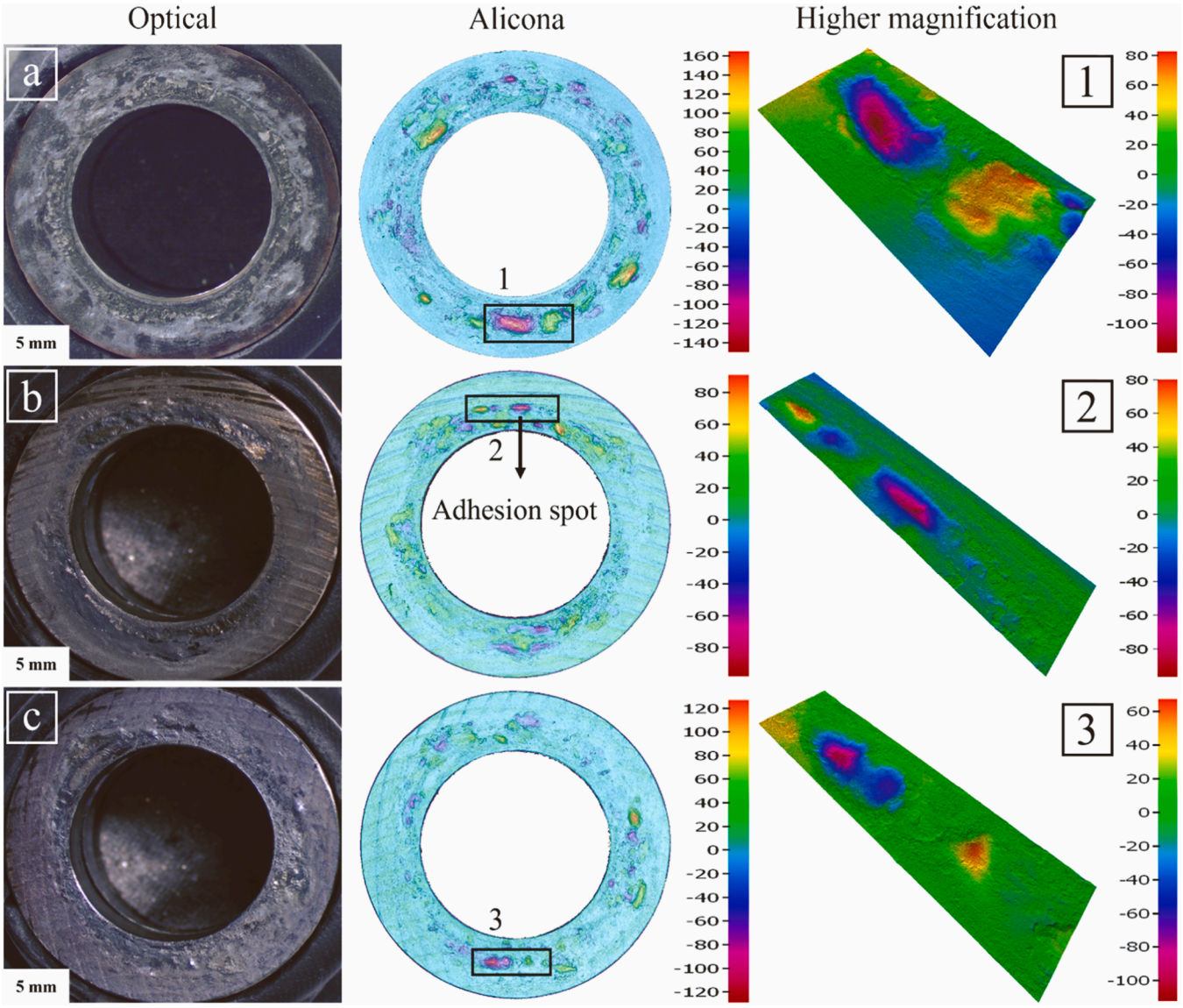

Fig. 7. Optical images and Alicona surface topography after gross sliding; (a) smooth, (b) parallel-oriented, and (c) perpendicular-oriented rough surfaces. (It should be noted that scales are in μm.).

instance; the accumulative frictional energy dissipation can be calculated by the areas inside fretting loops, and the friction evolution during test progress can be realized via their shapes [28]. Fig. 6 illustrates the friction evolution for the smooth and rough surfaces using the fretting loops at the specified load cycles. Several cycles in the running-in and steady-state conditions were selected to provide a thorough understanding of the frictional performance and fretting wear mechanism.

As shown, non-Coulomb friction (hook-shaped fretting loop) started after the start-up phase at the early stage of the test, and its maximum occurred at the COF peak for all the surfaces. This non-coulomb frictional behavior could be attributed to adhesive wear, arising from tangentially interlocked protrusions and depressions during the first few hundred (or thousand) load cycles [38]. This behavior was gradually alleviated by time, such that a relatively rectangular-shaped fretting loop and ideal Coulomb behavior were achieved after around 1×10^6 load cycles. Next, a minor impact was noted in the shape of the fretting loops by additional cycles, which implied a steady-state phase.

Fig. 7 represents the optical images and Alicona surface topography of the specimens after the gross sliding tests. The fine reddish-brown wear debris was expelled from both inner and outer contact edges, and the debris bed of the same color can evidently be seen on the fretted surfaces, confirming the entrapment of some wear particles, oxidation, and the formation of TBL. Third-body particles activate the velocity accommodation mechanism by decreasing the direct contact between the first bodies. Concerning the wear mechanism, it can be stated that all the damaged surfaces demonstrated a combination of adhesive and oxidative-abrasive wear, so the grey and reddish-brown sites are the signs of adhesion and oxidation, respectively. Adhesive wear is one of the most detrimental mechanisms, leading to subsurface damage, cracking, and early failure. Therefore, the most severe adhesion spots were selected for further surface and cross-sectional microscopic analyses, as marked in Fig. 7 with black rectangles.

The following issues are worth considering while examining the effect of surface texture and orientation on fretting scars:

1. The fretting damage level and its distribution on the surfaces can be used to validate the role of the new textured surface.
2. The most severely damaged areas in terms of size can be compared, given that fretting fatigue cracking is initiated there and results in subsequent fretting wear.

Fretting scars were more concentrated close to the inner edge, which

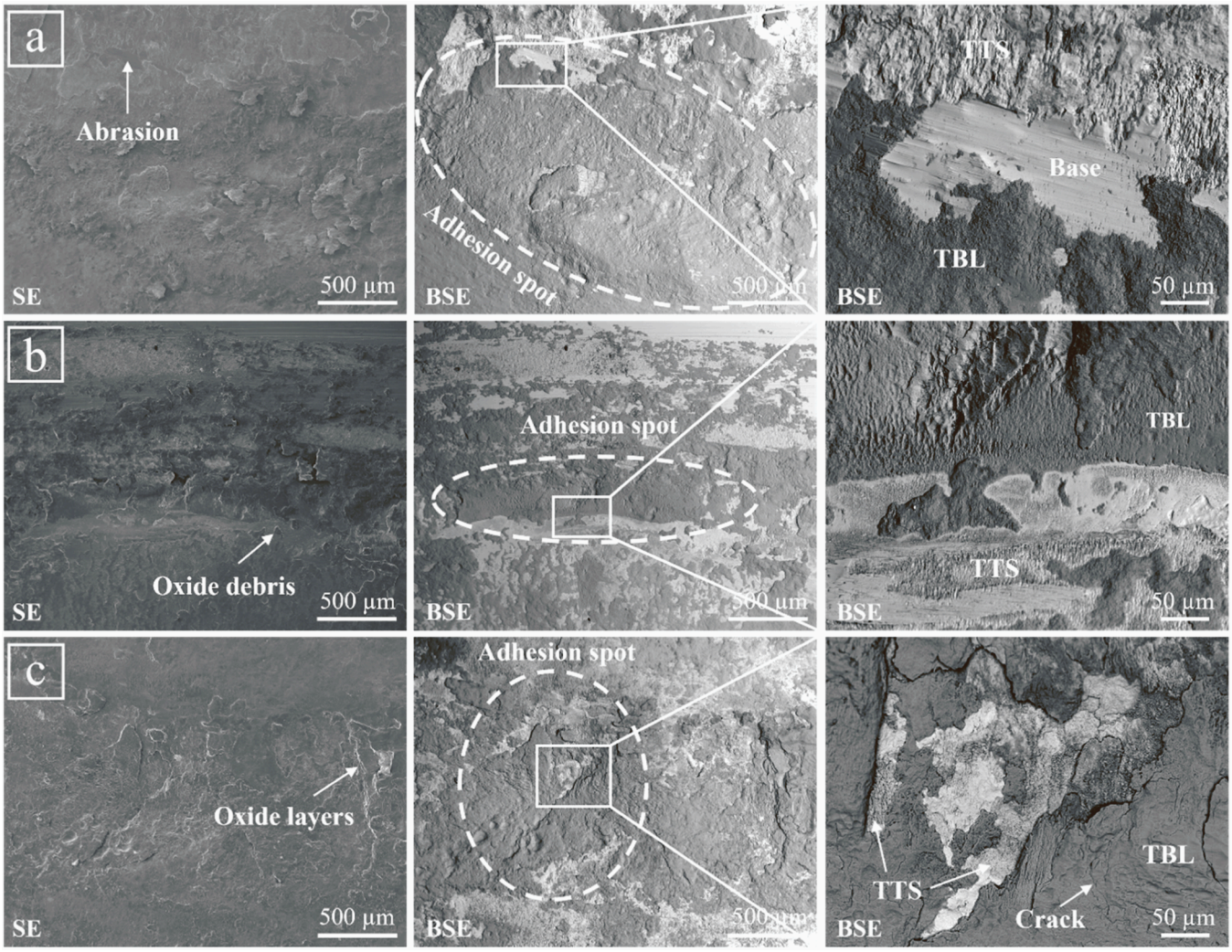

Fig. 8. Top-view SEM images of adhesion spots after gross sliding; (a) smooth, (b) parallel-oriented, and (c) perpendicular-oriented rough surfaces. (As indicated by SE and BSE, columns 1 and 2 present secondary and backscattered electron images from the same location, respectively.).

can be associated with a relatively higher normal pressure at the inner edge of the contact [28]. The traces of the grooves are visible on the fretted rough surfaces so that the parallel and perpendicular orientations can be discerned via the parallel curved lines and checked patterns on the surface, respectively. The millimeter-sized damaged spots were identified, which were most probably produced during the first few hundred or thousand cycles due to the initial adhesive wear. On the rough surfaces, the smaller area was initially subjected to fretting, and so the number and size of the adhesion spots were lower, attesting to its effective influence on fretting performance.

Compared to the surface profiles of the untested specimens (shown in Fig. 3), high protrusions and depressions after the fretting experiments indicate substantial tangential interlocking in the interface. It can be noticed in the form of a high adhesive friction peak at the early stage of the fretting test, causing remarkable material transfer between the contact bodies. Accordingly, the lower COF peaks in the rough surface cases can be an indication of lower fretting damage and milder adhesion spots on the surface. There was not a significant difference in the fretting scar levels of the two contact orientations, which agrees with their COF results. In other words, the tangentially interlocked spots can be linked to high non-Coulomb friction behavior at the early stage of the experiment as stated by Mulvihill et al. [38] and seen in the ΔCOF curves.

The SEM images of the selected adhesion spots are presented in Fig. 8 so that the areas circled in white signify their exact locations. The adhesion spots are almost covered with oxide layers, and their size is clearly smaller in rough cases. In the higher magnification SEM images, oxide layers (TBL) and unoxidized substrate can be distinguished. Besides, there is another area with a lower oxygen content than TBL and a needle-like microstructure, which may be attributed to tribologically transformed structure (TTS). Adhesive and oxidative-abrasive wear mechanisms can be better demonstrated by SEM images of the fretted surface using secondary electron (SE) and backscattered electron (BSE) images.

Fig. 9 illustrates the cross-sectional SEM images of the adhesion spots. The size was decreased in the following order: smooth, parallel, and perpendicular rough surfaces. Fretting degradation layers, including the TBL, TTS, and general deformation layer (GDL), were detected from the surface toward the base material for both surfaces in accordance with the literature [18]. These degradation layers were distinguished in the fretting wear investigation with Inconel 600 alloys and a ball-on-flat contact configuration by Li et al. [39].

Sauger et al. [40] proposed that the majority of the third body is generated through the cracking of the hard and brittle TTS under contact stresses, causing its milling into small particles. These particles can subsequently sinter back to the surface and form the TBL. A thick TBL is seen in the smooth case, which is fully cracked and porous. The parallel case also reveals a thick TBL, but it is more coherent and less cracked than that of the smooth one, spreading over larger areas in the adhesion

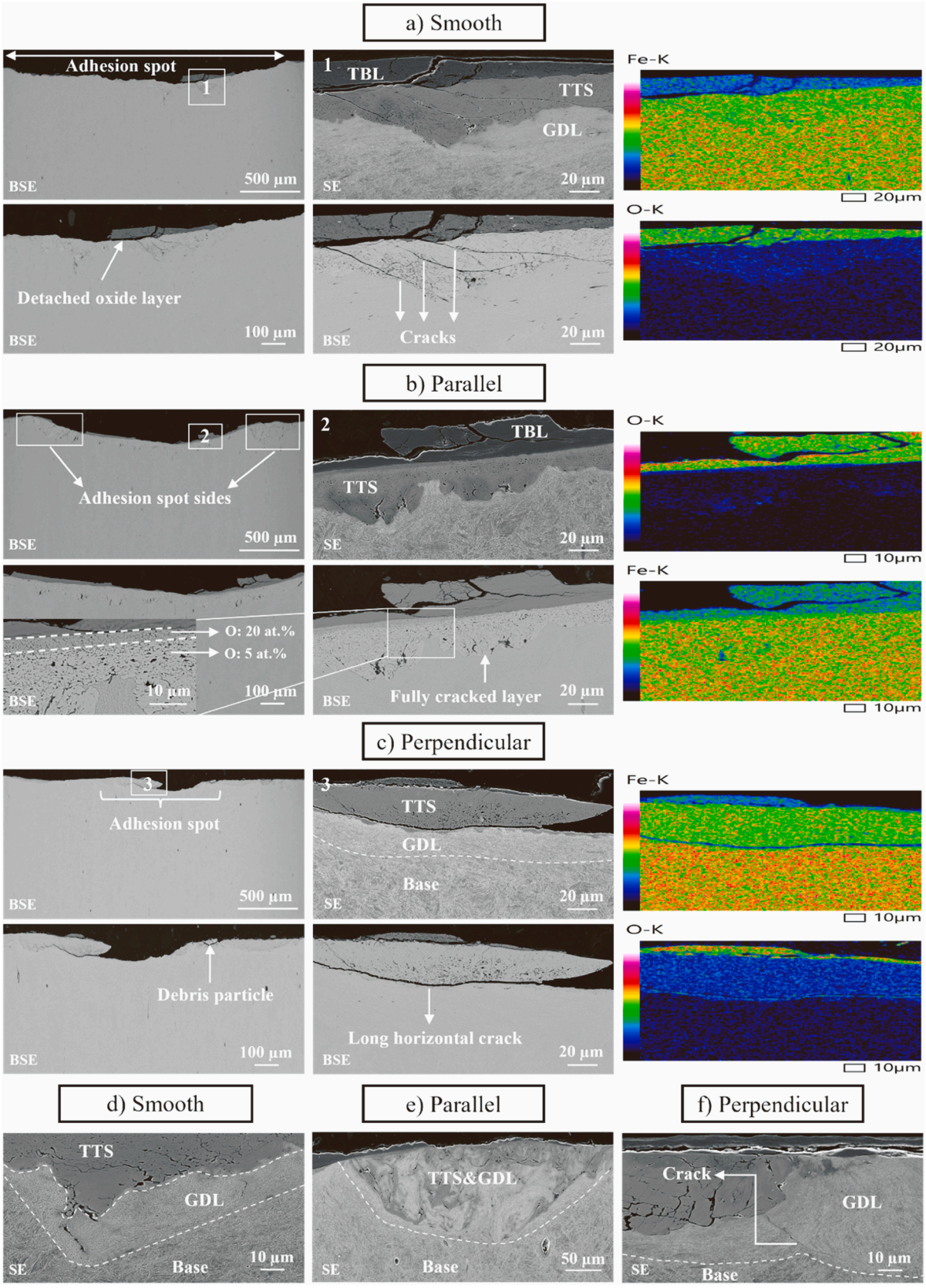

Fig. 9. Cross-sectional SEM images and EDS maps of adhesion spots after gross sliding.

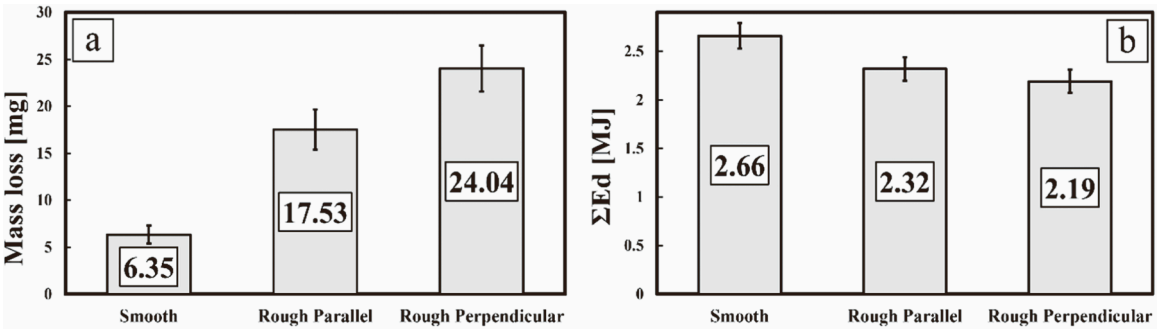

Fig. 10. (a) Mass loss due to fretting wear, and (b) the accumulated frictional energy dissipation after gross sliding.

spot. Two different types of TBL were identified as follows:

1. A highly porous layer, which supports the sintering theory and explains the formation of the pores by adhering non-compatible debris particles together to create a debris layer (Fig. 9a).
2. A non-porous TBL layer with long horizontal cracks, which seems more stable and adherent to the surface than the first type (Fig. 9b). A porous to non-porous transformation of oxide layer changed the approximate atomic ratio of Fe:O gained via EDS analysis from 45:55–35:65.

The oxidation rate and formation of TBL are influenced by the duration that third body particles remain loose in the interface, particle size, and ease of oxygen penetration through the confined area in the fretting contacts [40]. Hence, the coherent TBL on the rough surface can be ascribed to the presence of grooves, which facilitated oxygen transfer to the contact surface and led to a higher oxidation rate. Except a small and thin TBL of the first type in the center of the adhesion spot (Fig. 9c), the second type of TBL was noticed in the perpendicular case, which distributed thinly and flaking off the surface. It may indicate the difficulty of oxygen transfer to the center of adhesion spot because of the checked surface pattern shaped by positioning the grooves in a perpendicular orientation.

It has been reported [41] that the development of TTS is associated with exceeding the ultimate strain level of martensite. This hypothesis is highly reasonable because it is mostly observed in adhesion spots, where the plastic deformation level is markedly high, leading to strains beyond the ultimate threshold. TTS was identified as a densely cracked phase due to its hard and brittle characteristics. The main cracks propagated at an angle of 30–45° to the surface, as reported by the literature [18,41], branching out in various directions and extending through the structure. EDS maps confirmed a varying oxygen content (up to 20 at%) in TTS, which depended on its location; the closer to the surface, the higher the oxygen content. The high-magnification EDS images implied that this level of oxygen can be attributed to oxygen diffusion into TTS through a multitude of cracks. There were no major differences in its thickness, and in the perpendicular case, it detached from the surface by a long horizontal crack.

Owing to the severe plastic deformation of the material (which is required for cracking) caused by the contact stresses, the GDL region can be generated beneath TTS [42,43]. Moreover, this extensive material deformation reduced the grain size and oriented it parallel to the crack face. In the smooth and parallel-oriented cases, a mixed region of TTS and GDL was noticed at the side of the adhesion spots (Fig. 9e).

In the previous studies on the smooth surface with the same configuration and parameters, the high COF peak of roughly 1.4 caused by local contact stress concentration was noted as one of the fretting fatigue cracking sources in the adhesion spots [27]. This kind of cracking can even be observed in the rough cases with a lower COF peak, and the effect of COF peak removal on fretting fatigue cracking was studied using the partial slip regime later in this paper. The cracks propagated at an oblique angle to the contact interface and ranged in size from tens to hundreds of micrometers. The average crack lengths of 265, 135, and 70 μm and maximum crack lengths of 420, 240, and 130 μm were measured in smooth, parallel, and perpendicular rough surfaces, respectively. The longer cracks were mostly detected at the sides of adhesion spots in the GDL-TTS area for the smooth and parallel surfaces. The long horizontal cracks alongside TTS, as in the perpendicular-oriented rough case, are not as dangerous as the oblique cracks and were not counted. Furthermore, the network of the small cracks connected to each other in TTS was not included in the crack length analysis. In addition to the cracks within TTS and on the boundary of the GDL and TTS phases, the crack growth also continued toward the bulk in a few spots in the smooth and perpendicular cases (Fig. 9d, f).

The damage degree declined toward the sides of the adhesion spots and further away, and TBL was replaced with the thin layers of the sintered wear debris in the localized areas. Besides, the interface of the degradation layers is of significant importance to understanding their formation mechanisms. For instance, in spite of the porous and cracked appearance of TBL and TTS, they can easily be discerned with a distinct interface, which implies their microstructure differences. At the interfaces of TTS-GDL and GDL-base material, the gradual changes from one phase to another were caused by deforming plastically the undeformed martensite, flattening the grains directed to TTS, refining to a fine-grained structure, taking place the phase transformation from martensite to ferrite [40], cracking, and penetrating oxygen into the cracked TTS, respectively. The EDS maps (Fig. 9) illustrate the phase interfaces and also the oxygen penetration into TTS, particularly in the perpendicular case.

Based upon the Archard wear equation, sliding distance, normal force, and a constant (acquired from experiments and dependent on several parameters, e.g., surface quality) correlate linearly, while hardness is inversely proportional to wear rate [44]. All the above-mentioned parameters, except for the dimensionless constant (which varies due to different surface qualities), have the same nominal values in these tests. The wear mass loss of the fretted specimens was represented in Fig. 10a, and the maximum error of the mass measurements, which refers to the accuracy of weighing, was around 1 mg. The standard deviation of the measurements is shown in Fig. 10.

The markedly higher values were recorded in the rough case than in the smooth one. According to Berthier et al. [17], fretting wear is governed by wear particle ejection rather than particle formation. Therefore, the higher mass loss in the rough contact can be attributed to their surface texture. It can be argued that the grooves on the contacting surfaces made debris ejection easier and resulted in a higher rate of debris generation. In other words, the wear activation energy in the gross slip running condition was decreased by increasing the surface roughness, leading to a higher wear rate in the rough surfaces compared to the smooth ones [21]. As Varenberg et al. asserted, the presence of pores on the contacting surface improved the ejection of wear particles by creating spaces for wear debris accumulation [45]. As a result, the

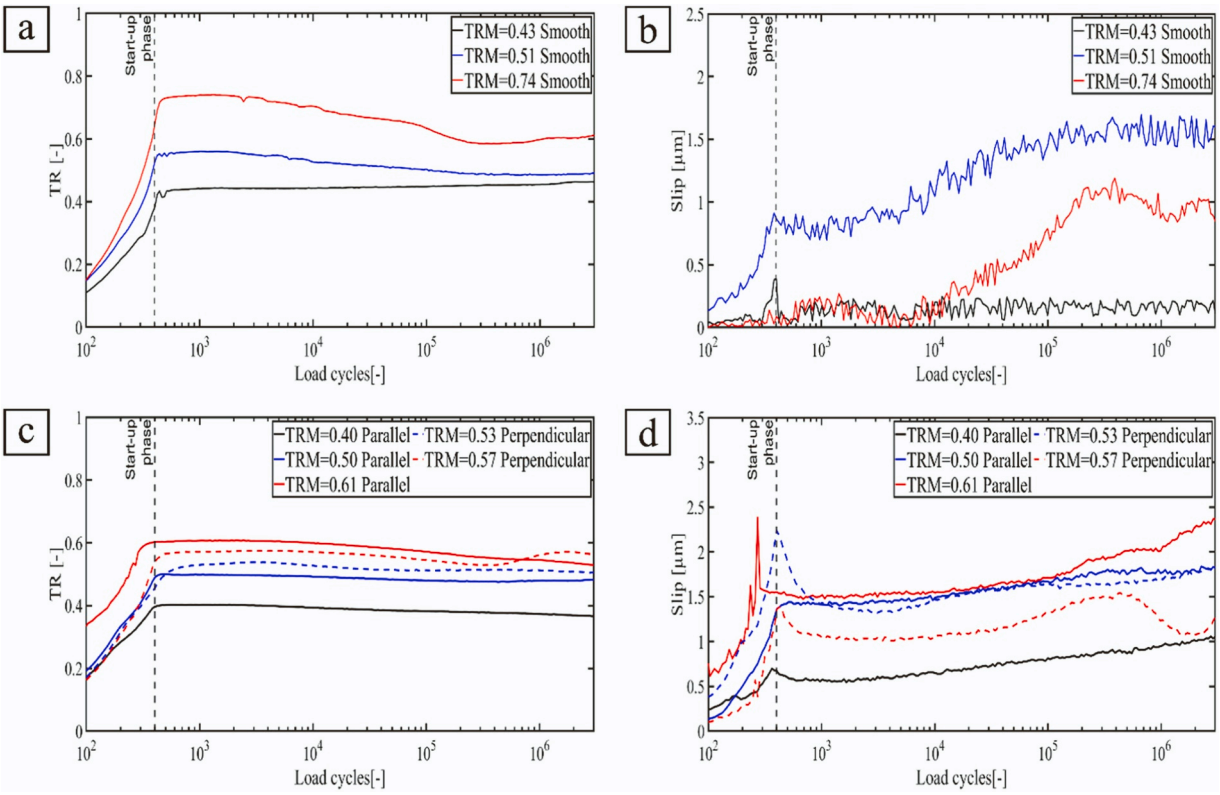

Contact	Smooth			Parallel			Perpendicular	
TRM level	0.43	0.51	0.74	0.40	0.50	0.61	0.53	0.57
Accumulated sliding distance (m)	0.48	20.11	10.82	11.72	21.60	26.09	21.00	14.83

Fig. 11. (a,c) TR and (b,d) slip amplitude in the stable friction tests.

microgeometry of surface can significantly influence on the wear rate.

The correlation between the accumulated frictional energy dissipation and fretting wear, based on the assumption of easy ejection of wear particles, was reported by researchers [46,47]. Fig. 10b shows an unexpected opposite trend to wear mass loss despite the minor difference in the energy dissipated by the frictional force between the contacting bodies. Indeed, wear can be expected to intensify with a rise in dissipated frictional energy if this energy is spent producing wear particles that can later be ejected from the contact. Nevertheless, our data were in direct contradiction. Therefore, it can be assumed that the frictional energy in the smooth case was dissipated more to overcome adhesion (in consequence of the high COF peak) or in the velocity accommodation mechanism, rather than contributing to wear. In addition, the frictional energy may have caused the particle detachment, but it could not lead to ejection from the interface as much as what happened with the rough textured surfaces. The higher wear mass loss and lower dissipated energy in the perpendicular case, compared with the parallel one, might be attributed to the larger areas of the grooves between the contact bodies, resulting in more debris ejection followed by increased debris formation. It should be considered that debris ejection is more challenging in a large flat-on-flat contact than in a small Hertzian contact. All in all, the lower COF and more severe fretting wear in the rough cases than in the smooth ones are in line with the literature on the influence of the initial surface roughness on fretting, as mentioned in the introduction section [21–23].

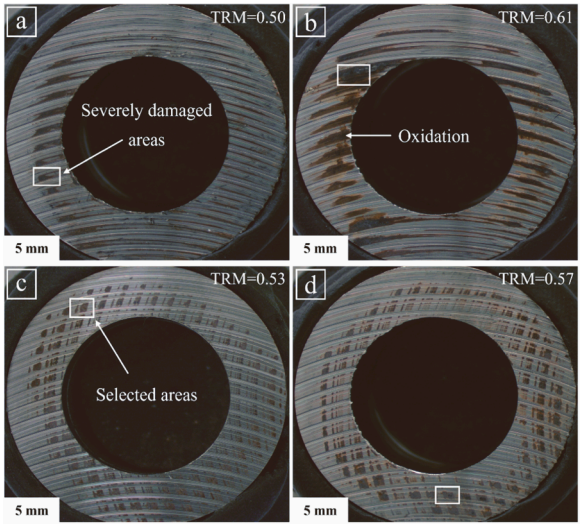

Fig. 12. Optical images of the fretting scars after the stable friction tests; (a,b) parallel-oriented and (c,d) perpendicular-oriented rough surfaces.

3.2. Stable friction tests

In this test series, a portion of the frictional force was used in the stick and partial slip conditions to achieve stable friction behavior throughout the experiment, and a detailed explanation of the stable friction test was provided in the literature [28,48]. The fretting tests were executed with tangential displacement-controlled loading, and the slip amplitude was calculated based on the zero-torque-based rotation amplitude.

Fig. 11 exhibits the TR and slip curves for both the smooth [28] and rough surfaces. The friction behavior is considered stable if the smooth

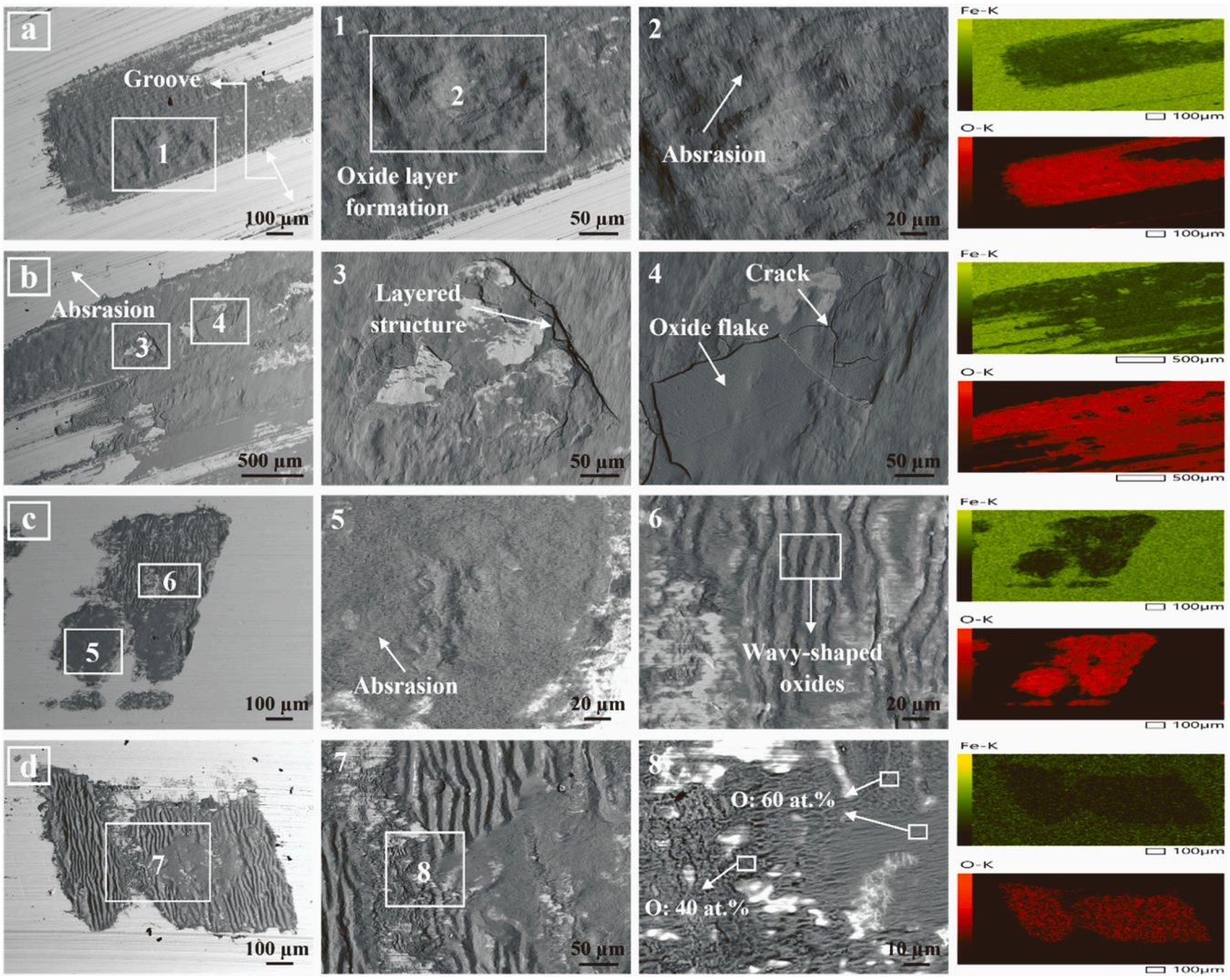

Fig. 13. Top-view SEM-BSE images and EDS maps of the fretting scars after the stable friction tests; (a,b) parallel-oriented, and (c,d) perpendicular-oriented rough surfaces.

line can be seen in the TR curves without substantial peaks or variations. Indeed, the goal was to avoid any instability in the frictional load that could result in adhesion between the material pairs.

A roughly similar threshold of about 0.5 was attained for the rough surface as that of the smooth one. The smooth TR lines are identified up to the threshold except for a minor decreasing trend in TR values as the slip slightly rises. By increasing TR above the threshold, TR curves indicate higher values at the initial stage and then reduce, showing a similar trend to that of gross sliding, which is divided into the maximum and stabilized COF. The higher the TRM, the more unstable frictional behavior is distinguished in the fretting tests. Additionally, there was no considerable difference between the two contact orientations.

As presented in Fig. 11b, d, the limited use of frictional force resulted in a few micrometers of slip in the interface. In the stable TR zone, some slip occurred all the time for the rough cases, while there was nearly zero slip (or stick) for the smooth ones. Besides, higher slips were gained for the rough contacts compared to the smooth ones at nearly the same TR level.

Fig. 12 reveals that some parts of the contact area experienced slip and surface damage, while the other parts were stuck and remained intact. This observation elucidated that the surface was under a partial slip regime. Notably, less severe damage occurred in these small slip amplitude tests than in the gross sliding conditions.

Oxidative-abrasive was the only fretting wear mechanism intensified by increasing TR values. A rise in TR developed the damaged area and the severity of fretting scars on the surface. Also, the influence of the TR level on the fretting damage was more pronounced in the parallel case. The small and individual contact areas in the perpendicular case led to the small damaged spots and thus lower surface damage such that fretting scars were generally milder than in the parallel case. All in all, no adhesion spot was noticed on the surfaces, which can be interpreted by the easier oxidation as a result of the grooves inducing abrasive wear rather than adhesive wear.

Fig. 13 displays SEM images and corresponding EDS maps of the most severely damaged areas marked by the white rectangles in Fig. 12. The fretting scars were mostly initiated at the edges of the grooves, which were one of the local stress concentration sites and the nearest regions in the oxygen penetration path. The larger damaged spots can be found in the parallel orientation.

The existence of the oxide layers on the surfaces was corroborated through SEM-EDS studies, with no indication of adhesive wear. In addition, a distinctive wavy shape of the oxidized layers is noticed in the perpendicular orientation, which can be explained by the contact patterns and oscillatory fretting motion. In the parallel-oriented rough surfaces above the TR threshold, the higher magnification SEM images (Fig. 13b) clearly reveal a layered structure of oxide flakes on the

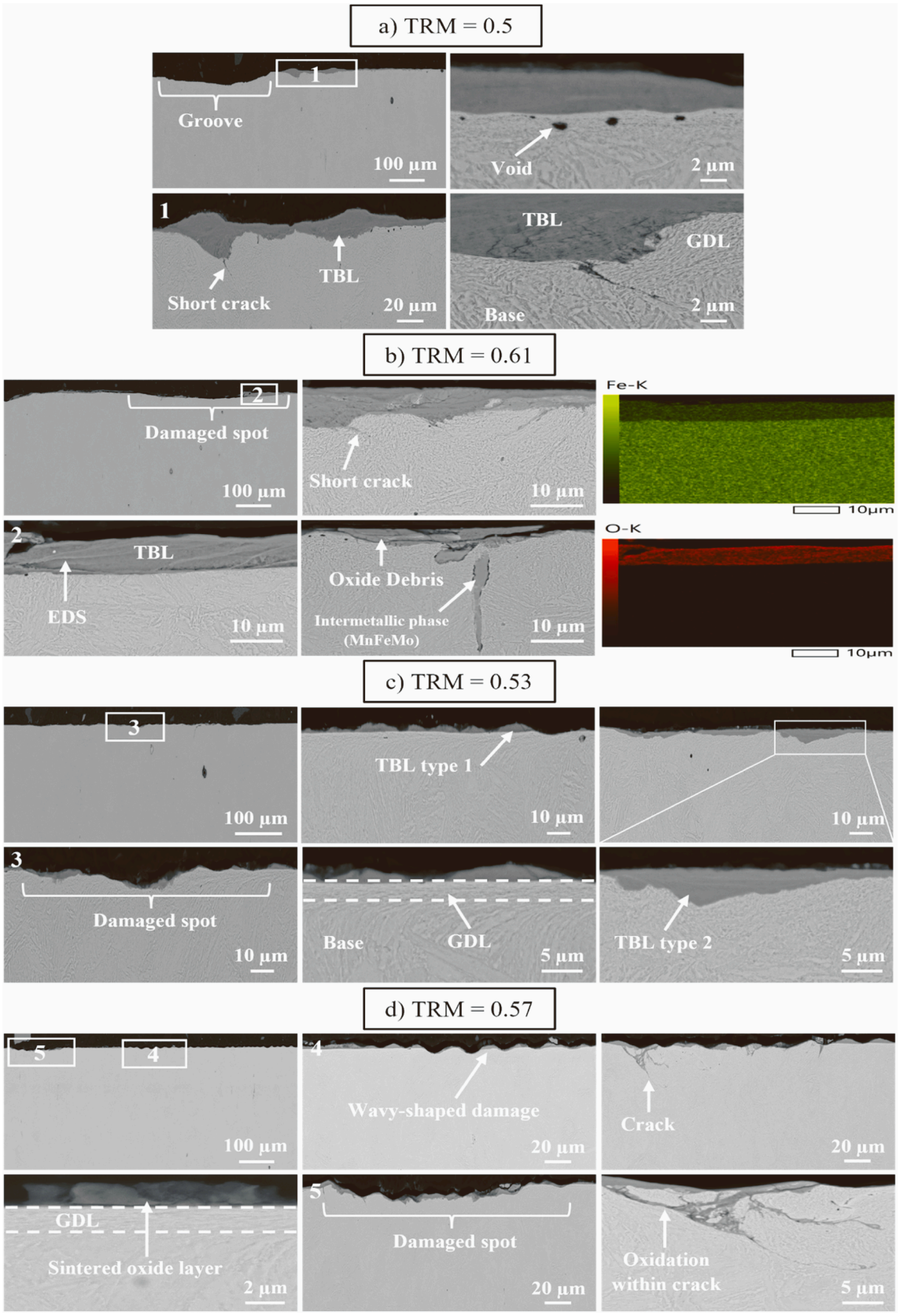

Fig. 14. Cross-sectional BSE-SEM images and EDS maps of the fretting scars after the stable friction tests; (a,b) parallel-oriented, and (c,d) perpendicular-oriented rough surfaces.

surface, which were cracked and broken as a result of the high hardness and brittle nature of iron oxide. Moreover, the scratches on the piled-up oxides and base material in fretting scars indicate the abrasive wear mechanism in all the tests.

Fig. 14 illustrates the cross-sectional SEM images and corresponding EDS maps of the selected fretting scars. TBL and GDL are the only degradation layers present, and there is no indication of TTS, which is consistent with the QT-QT smooth case in the previous study [27]. The higher the TR, the more TBL coverage was seen on the surface for both contact orientations. However, this amount of TBL was considerably less than in gross sliding. More oxidation and TBL were discerned for the rough surface compared to the smooth one, despite having approximately the same level of TR. The higher TR value causes the higher local contact stresses, which leads to more severe protrusions and depressions. Two different types of TBL were recognized, the first of which was an oxide layer attached to the surface. But for the second type, it can be postulated that the oxidized structure penetrated the surface (Fig. 14c).

Thin GDL layers can be detected, and the higher the TR, the thicker the GDL becomes. Overall, GDL layers included lower thicknesses in the perpendicular orientation than in the parallel one. Larger damaged areas were observed for the parallel orientation. On the same scale, it featured one large damaged spot, whereas the perpendicular one had several small damaged spots.

No cracks occurred in the parallel orientation below the TR threshold with a TRM value of 0.4 and a slip amplitude of less than 1 μm. Around the threshold, the crack pairs were not formed, and only one individual crack appeared with a length of 10 μm in the parallel case with a TRM of 0.5, while no visible cracks were found in the perpendicular one with a TRM of 0.53. Cracks enhanced in length and number after crossing the threshold, which resulted in maximum crack lengths of 23 μm and 42 μm in the parallel and perpendicular cases, respectively. Furthermore, the average crack lengths were estimated at 20 μm and 15 μm in the parallel and perpendicular orientations, respectively. The noticeably shorter cracks were identified in comparison to gross sliding, as adequate friction and slip are required for crack propagation. Moreover, it should be considered that all the results were obtained from one cross-section, and a more comprehensive view of fretting fatigue cracks can be gained by analyzing more cross-sections.

Regarding fretting wear debris, slip amplitude was less than 2.5 μm for the stable friction tests, and minor fretting damage can be seen on the surfaces (Fig. 12). In fact, there was no collectible debris during the fretting test. Debris was ejected from the interface in the gross sliding tests, but this research investigated the frictional behavior (COF and TR) of the smooth-smooth and rough-rough contacts, together with the surface and cross-sectional damage characterization in the adhesion spots. Thus, examining debris, which is usually generated as a result of oxidative-abrasive wear, was not the main purpose. However, the study of wear debris can be a beneficial addition to future research.

4. Conclusions

A large annular flat-on-flat contact device was employed to experimentally evaluate the fretting behavior of quenched and tempered steel. It aimed to assess a rough surface with a particular texture in parallel and perpendicular contact orientations and compare the results with those of a ground surface. Experiments were conducted in partial slip to attain a stable friction threshold and in gross sliding to recognize the COF peak and fretting damage. The following conclusions were drawn:

- In gross slip, average COF peaks of 1.35, 1.15, and 1.05 occurred after 379, 4423, and 5270 cycles in the smooth, parallel, and perpendicular rough cases, respectively. However, COF reached nearly 0.7 in the steady-state step for both surface textures and contact orientations.
- More and larger adhesion spots appeared on the smooth surface, and both cases showed all three fretting-induced degradation layers. Specifically, the average crack lengths measured 265 μm for smooth, 135 μm for parallel rough, and 70 μm for perpendicular rough cases, while the maximum crack lengths were 420, 240, and 130 μm, respectively.
- It can be assumed that the easier debris ejection and contact oxygenation due to the grooves on the rough surface alleviated adhesive wear and activated oxidative-abrasive wear at the early stage, causing a lower COF peak and less fretting-induced damage and cracking.
- The rough surface indicated a significantly higher wear mass loss, whereas the accumulated frictional energy dissipation was lower. It can be stated that its surface texture may facilitate wear particle ejection, governing the total mass loss. Also, a higher COF peak in the smooth surface can cause higher dissipated energy to overcome adhesion instead of contributing to wear.
- In partial slip, the threshold of 0.5 for stable frictional behavior was achieved in both cases. Oxidation-abrasion as the only wear mechanism was reduced in the perpendicular-oriented contact. No tribologically transformed structure was noted in the stable friction tests. The cross-sectional cracks were not detected below and around the threshold in the parallel and perpendicular orientations, respectively. The higher the traction ratio, the longer the cracks; the longest crack of nearly 42 μm was related to the perpendicular-oriented contact.

Declaration of Competing Interest

The authors declare that they have no known competing financial interests or personal relationships that could have appeared to influence the work reported in this paper.

Data Availability

Data will be made available on request.

Acknowledgment

The authors express their special thanks of gratitude to emeritus Prof. A. Lehtovaara, the former supervisor of this research. The authors appreciate the financial support provided by Business Finland Oy (formerly Tekes) in the form of research project ISA (Dnro 7204/31/2018). Also, We would like to thank Tampere Microscopy Center for their SEM instrument and assistance.

Statement of originality

Authors hereby certify that the content of this manuscript is original and has not been published or submitted for publication anywhere else.

References

[1] Hintikka J, Juoksukangas J, Lehtovaara A, Frondelius T, Mäntylä A. Non-idealities in fretting contacts. J Struct Mech 2017;50:171–4.
[2] Hills DA, Nowell D. Mechanics of fretting fatigue. Dordrecht: Kluwer Academic Publishers; 1994.
[3] Waterhouse RB. Fretting corrosion. ISBN 0 08 16902. Oxford: Pergamon Press; 1972.
[4] Johnson KL. Contact mechanics. Cambridge: Cambridge University Press; 1985.
[5] Wallace JM, Neu R. Fretting fatigue crack nucleation in Ti–6Al–4V. Fatigue Fract Eng Mater Struct 2003;26:199–214.
[6] Mäntylä A, Hintikka J, Frondelius T, Vaara J, Lehtovaara A, Juoksukangas J. Prediction of contact condition and surface damage by simulating variable friction coefficient and wear. Tribol Int 2020;143:106054.
[7] Hintikka J, Lehtovaara A, Mäntylä A. Non-Coulomb friction in gross sliding fretting conditions with aluminium bronze against quenched and tempered steel. Tribol Int 2014;79:151–61.
[8] Hirsch MR, Neu RW. Fretting damage in thin sheets: analysis of an experimental configuration. Tribol Int 2011;44:1503–10.

[9] Hintikka J, Lehtovaara A, Mäntylä A. Normal displacements in non-Coulomb friction conditions during fretting. Tribol Int 2016;94:633–9.
[10] Hintikka J, Lehtovaara A, Lönnqvist C. Effect of start-up schemes and amplitude of tangential motion on friction behavior in fretting point contact. Tribol Int 2011;44:1535–43.
[11] Hintikka J, Lehtovaara A, Mäntylä A. Fretting-induced friction and wear in large flat-on-flat contact with quenched and tempered steel. Tribol Int 2015;92:191–202.
[12] Hintikka J, Lehtovaara A, Mäntylä A. Third particle ejection effects on wear with quenched and tempered steel fretting contact. Tribol Trans 2017;60:70–8.
[13] Madge JJ, Leen SB, McColl IR, Shipway PH. Contact-evolution based prediction of fretting fatigue life: Effect of slip amplitude. Wear 2007;262:1159–70. 2007.
[14] McColl IR, Ding J, Leen SB. Finite element simulation and experimental validation of fretting wear. Wear 2004;256:1114–27.
[15] Madge J, Leen S, McColl I, Shipway P. Contact-evolution based prediction of fretting fatigue life: effect of slip amplitude. Wear 2007;262:1159–70.
[16] Godet M. The third-body approach: a mechanical view of wear. Wear 1984;100:437–52.
[17] Berthier Y, Vincent L, Godet M. Velocity accommodation in fretting. Wear 1988;125:25–38.
[18] Nurmi V, Hintikka J, Juoksukangas J, Honkanen M, Vippola M, Lehtovaara A, Mäntylä A, Vaara J, Frondelius T. The formation and characterization of fretting-induced degradation layers using quenched and tempered steel. Tribol Int 2019;131:258–67.
[19] Bruzzone AAG, Costa HL, Leonardo PM, Lucca DA. Advances in engineered surfaces for functional performance. CIRP Ann Technol 2008;57:750–69.
[20] Vázquez J, Navarro C, Domínguez J. Analysis of the effect of a textured surface on fretting fatigue. Wear 2013;305:23–35.
[21] Kubiak KJ, Liskiewicz TW, Mathia TG. Surface morphology in engineering applications: influence of roughness on sliding and wear in dry fretting. Tribol Int 2011;44:1427–32.
[22] Kubiak KJ, Mathia TG. Influence of roughness on contact interface in fretting under dry and boundary lubricated sliding regimes. Wear 2009;267:315–21.
[23] Kubiak KJ, Mathia TG, Fouvry S. Interface roughness effect on friction map under fretting contact conditions. Tribol Int 2010;43:1500–7.
[24] Warmuth AR, Pearson SR, Shipway PH, Sun W. The effect of contact geometry on fretting wear rates and mechanisms for a high strength steel. Wear 2013;301:491–500.
[25] Beheshti A, Aghdam AB, Khonsari MM. Deterministic surface tractions in rough contact under stick–slip condition: application to fretting fatigue crack initiation. Int J Fatigue 2013;56:75–85.
[26] Qin W, Jin X, Kirk A, Shipway PH, Sun W. Effects of surface roughness on local friction and temperature distributions in a steel-on-steel fretting contact. Tribol Int 2018;120:350–7.
[27] Juoksukangas J, Nurmi V, Hintikka J, Vippola M, Lehtovaara A, Mäntylä A, Vaara J, Frondelius T. Characterization of cracks formed in large flat-on-flat fretting contact. Int J Fatigue 2019;124:361–70.
[28] Hintikka J, Mäntylä A, Vaara J, Frondelius T, Lehtovaara A. Stable and unstable friction in fretting contacts. Tribol Int 2019;131:73–82.
[29] Juoksukangas J, Nurmi V, Hintikka J, Honkanen M, Vippola M, Lehtovaara A, Mäntylä A, Vaara J, Frondelius T. Cracks and degradation layers in large flat-on-flat fretting contact with steels and cast iron. Tribol Int 2020;145:106102.
[30] Leidich E, Maiwald A, Vidner J. A proposal for a fretting wear criterion for coated systems with complete contact based on accumulated friction energy density. Wear 2013;297:903–10.
[31] Iwabuchi A. The role of oxide particles in the fretting wear of mild steel. Wear 1991;151:301–11.
[32] Juoksukangas J, Hintikka J, Lehtovaara A, Mäntylä A, Vaara J, Frondelius T. Avoiding the initial adhesive friction peak in fretting. Tribol Int 2020;460:203353.
[33] Berthier Y, Godet M, Brendle M. Velocity accommodation in friction. Tribol Trans 1989;32:490.
[34] Fouvry S, Arnaud P, Mignot A, Neubauer P. Contact size, frequency and cyclic normal force effects on Ti–6Al–4V fretting wear processes: an approach combining friction power and contact oxygenation. Tribol Int 2017;113:460–73.
[35] Baydoun S, Fouvry S. An experimental investigation of adhesive wear extension in fretting interface: application of the contact oxygenation concept. Tribol Int 2020;147:106266.
[36] Baydoun S, Arnaud P, Fouvry S. Modelling adhesive wear extension in fretting interfaces: an advection-dispersion-reaction contact oxygenation approach. Tribol Int 2020;151:106490.
[37] Baydoun S, Arnaud P, Fouvry S. Modeling contact oxygenation and adhesive wear extension in axisymmetric flat circular fretting interfaces. Wear 2021;477:203822.
[38] Mulvihill DM, Kartal ME, Olver AV, Nowell D, Hills DA. Investigation of non-Coulomb friction behaviour in reciprocating sliding. Wear 2011;271:802–16.
[39] Li J, Lu Y, Zhang H, Xin L. Effect of grain size and hardness on fretting wear behavior of Inconel 600 alloys. Tribol Int 2015;81:215–22.
[40] Sauger E, Fouvry S, Ponsonnet L, Kapsa P, Martin J, Vincent L. Tribologically transformed structure in fretting. Wear 2000;245:39–52.
[41] Sauger E, Ponsonnet L, Martin J, Vincent L. Study of the tribologically transformed structure created during fretting tests. Tribol Int 2000;33:743–50.
[42] Basseville S, Cailletaud G. An evaluation of the competition between wear and crack initiation in fretting conditions for Ti–6Al–4V alloy. Wear 2015;328:443–55.
[43] Jeung H, Kwon J, Lee CY. Crack initiation and propagation under fretting fatigue of Inconel 600 alloy. J Mech Sci 2015;29:5241–4.
[44] Archard JF. Contact and rubbing of flat surfaces. J Appl Phys 1953;24:981–8.
[45] Varenberg M, Halperin G, Etsion I. Different aspects of the role of wear debris in fretting wear. Wear 2002;252:902–10.
[46] Fouvry S, Kapsa P, Vincent L. Quantification of fretting damage. Wear 1996;200:186–205.
[47] Fouvry S, Duó P, Perruchaut P. A quantitative approach of Ti–6Al–4V fretting damage: friction, wear and crack nucleation. Wear 2004;257:916–29.
[48] Hintikka J, Lehtovaara A, Frondelius T, Mäntylä A. Tangential traction instability in fretting contact below fully developed friction load. J Struct Mech 2017;50:175–8.